# Title: Nigro-striatal dopamine activation lowers behavioral and neuronal phenotypes associated with obsessive-compulsive disorder

**Authors:** Agata Casado-Sainz[1]†, Frederik Gudmundsen[1]†, Simone L. Baerentzen[1], Denise Lange[2], Annemette Ringsted[1], Isabel Martinez-Tajada[1], Siria Medina[1], Hedok Lee[3], Claus Svarer[1], Sune H. Keller[4], Martin Schain[1], Celia Kjaerby[5], Patrick M. Fisher[1], Paul Cumming[6,7], Mikael Palner[1]*

**Affiliations:**

[1] Neurobiology Research Unit, Copenhagen University Hospital, Copenhagen, Denmark

[2] Institute of Aerospace Medicine, German Aerospace Center (DLR), Cologne, Germany.

[3] Department of Anesthesiology and Pediatric Anesthesiology, Yale University, New Haven, CT, United States

[4] Department of Clinical Physiology, Nuclear Medicine and PET, Copenhagen University Hospital, Copenhagen, Denmark

[5] Center for Translational Neuromedicine, University of Copenhagen, Copenhagen, Denmark

[6] Department of Nuclear Medicine, Inselspital, Bern University, Bern, Switzerland

[7] School of Psychology and Counselling, Queensland University of Technology, Brisbane, Australia

† These authors contributed equally to the publication

* Corresponding author, mikael.palner@nru.dk

Neurobiology Research Unit

6-8 Inge Lehmanns Vej

Rigshospitalet, buil. 8057

DK-2100 Copenhagen, Denmark
Phone: +45 9399 6712

**One Sentence Summary:** Chemogenetic nigro-striatal dopamine activation modulates functional connectivity and behaviors related to cortico-striato-thalamo-cortical circuit – perspectives for the treatment of obsessive-compulsive disorder.

**Abstract:** Nigro-striatal dopamine transmission in the rat dorsomedial striatum (DMS) engages the cortico-striato-thalamo-cortical (CSTC) circuit. Modulation of the CSTC circuit can emulate behavioral and functional aspects of neuropsychiatric diseases, including obsessive compulsive disorder (OCD). Classical pharmacological and neurotoxic manipulations of brain circuits suffer from various drawbacks related to off-target effects and adaptive changes. Chemogenetics, on the other hand, enables a highly selective targeting of specific neuronal populations. In this study, we developed a chemogenetic method for selective activation of dopamine neurons innervating the rat DMS, and used this approach to investigate effects of targeted dopamine activation on CSTC circuit function. We monitored behavioral effects on locomotion, self-grooming, and prepulse inhibition of the startle response, which are stereotypic behaviors related to OCD, as well as effects on metabolic functional connectivity measured by [$^{18}$F]FDG PET, and regional concentrations of neurochemicals (i.e., glutamate, glutamine, N-acetylaspartate and N-acetylaspartateglutamate) measured by MR spectroscopy. We found that chemogenetic induced nigro-striatal dopamine transmission lowers some of the stereotypic behaviors that are considered hallmarks of OCD. It also disrupts functional connectivity between cortical areas and striatum, and increased total glutamate and N-acetylaspatateglutamate in cortical regions. The results thus establishes the importance of nigro-striatal dopamine transmission in modulation of CSTC function and emphasize DMS dopamine as a possible target for treatment of related neuropsychiatric disorders.

**Key words**: dopamine, cortico-striato-thalamo-cortical circuit, chemogenetics, DREADD, obsessive compulsive disorder, basal ganglia, [$^{18}$F]FDG PET, MR spectroscopy, glutamate.

## Introduction

The cortico-striato-thalamo-cortical (CSTC) circuit consists of neuronal pathways connecting the basal ganglia with frontal cortex, which conceptually mediates go/no-go signalling in response to stimuli. In simplified terms, CSTC circuit activation arising in the frontal cortex with projections to the dorsal striatum, where direct (go) and indirect (no-go) output pathways relay signals to the thalamus via the substantia nigra pars reticulata (SNr). The thalamus then communicates the processed signal back to cortex to complete the circuit (1, 2). Nigro-striatal dopamine projections modulate the CSTC circuit by inputs to spiny projection neurons (SPNs) in the dorsal striatum ,where SPNs expressing dopamine $D_1$ receptors directly innervate the SNr and SPNs expressing $D_2$ receptors indirectly innervate the SNr via relays in the globus pallidus and subthalamic nucleus (3, 4). Dysfunctions within the CSTC circuit are implicated in the etiologies of several neuropsychiatric diseases such as obsessive compulsive disorder (OCD) (2), Tourette's syndrome *(5)* and schizophrenia *(6)*. Interestingly, these diseases have overlapping behavioral phenotypes including tics, obsessions, compulsions, and sensory gating deficits.

Modulation of activity within the CSTC circuit by various techniques such as optogenetics, chemogenetics, transcranial direct current stimulation (tDCS), and deep brain stimulation can alter stereotypic and goal-directed behavior as well as sensory gating in rodents *(7–9)*, non-human primates *(10, 11)*, and humans *(12)*. [$^{18}$F]FDG PET investigations of the CSTC circuit in people with OCD using have shown hyperactivity in the orbito-frontal cortex (OFC) and anterior cingulate cortex (ACC), and increased metabolic connectivity from frontal cortex to the caudate *(13–16)*, which is the equivalent of the dorsomedial striatum (DMS) in rodents *(17)*. MR spectroscopy studies of people with OCD have shown relatively reduced total glutamate+glutamine (Glx) and N-acetylaspartate levels in cortical regions *(18–20)*. While clinical imaging studies thus suggest the presence of phenotypic characteristics of OCD, it is often difficult to establish causal relationships based on imaging results without having a direct way to target specific neuronal pathways.

The effects of dopamine signaling on CSTC functioning have been tested in animal studies using neurochemical lesions *(21, 22)*, and focal stereotaxic drug injections *(23)*. These methods, in varying degrees, bring unintended perturbations or adaptative changes of the nervous system. Recent years have seen the emergence of chemogenetics, in which transfection of Designer Receptors Exclusively Activated by Designer Drugs (DREADD) renders target neurons sensitive to G-protein coupled activation/inactivation following injection of an exogenous ligand, such as clozapine N-oxide (CNO) *(24)*. By enabling highly selective and reversible activation of specific neuronal subtypes and pathways, chemogenetics presents a powerful alternative to the classical pharmacological manipulations described above.

In this study, we apply selective chemogenetic activation of the DMS dopamine projections arising from the medial substantia nigra pars compacta (mSNpc) to test effects on behavioral,

functional, and molecular outcomes of thus perturbing the CSTC circuit of the rodent brain. We hypothesized that selective activation of dopaminergic projections to the DMS in normal rats would reduce behaviors resembling a compulsive phenotype (e.g., enhance sensory gating and lower grooming behavior). Furthermore, we predicted that this selective stimulation would have a top-down effect on cortico-striatal functional connectivity, as well as energy metabolism and glutamate concentrations in the frontal cortex and dorsal striatum as measured *in vivo*.

The experiment was designed in three phases (Fig. S1): (1) validation of the novel transfection approach, which selectively targets the nigro-striatal dopamine neurons innervating the DMS, (2) behavioral analyses following chemogenetic activation of these neurons, and (3) *in vivo* imaging of its effects on metabolic activity, functional connectivity and neurochemical markers in DMS and frontal cortex. We use immunohistochemical methods to confirm the targeted transfection, and behavioral testing to confirm locomotor activation in the transfected rats upon dopamine stimulation. In the first cohort of rats, we tested the behavioral effects of chemogenetic activation on self-grooming and sensory gating. In a second cohort of rats, we performed molecular imaging with [$^{18}$F]FDG-PET to map the brain-wide metabolic effects of chemogenetic activation, and MRS to map effects on neurochemical levels, specifically glutamate, glutamine and N-acetylaspartate. These results served to assess the influence of nigro-striatal dopaminergic activation on behavior, functional connectivity, and neurochemical levels related to CSTC circuit function.

## Results

### *Selective chemogenetic targeting of nigro-striatal dopaminergic projections*

Injection of Cre-dependent serotype 6 adeno associated viruses in the DMS of TH:Cre LE rats lead to selective retrograde expression of the mCherry reporter gene in dopaminergic projections arising from the mSNpc (Fig 1, A and B). Immunohistochemical identification of the mCherry reporter gene showed excellent selectivity towards the target neurons. Two different viral vectors were injected into the DMS, one carrying a Gq-coupled DREADD (DS-DQ: AAV6-hSyn-DIO-mCherry-hM3D(Gq)-WPRE) and the other vehicle vector without DREADD (DS-VEH: AAV6-hSyn-DIO-mCherry-WPRE) (Figure 1D). The staining intensity and spread from the injection site confirmed a highly reproducible target engagement in the DMS (Suppl. Fig. 2A). As expected, the larger DQ vector had a lower transfection ratio and decreased spread when compared to the VEH vector (Suppl. Fig. 2, C and D). There was no evident transfection of cell bodies in the DMS, nor of non-TH:Cre positive cells in the mSNpc (Fig. 1, E-J). Notably, the ventral tegmental area was also devoid of any mCherry-expressing cell bodies (Fig. 1, E,G and I).

*Nigro-striatal dopaminergic stimulation increases exploratory behaviors and lowers self-grooming*

We assessed rat behavior in an open field. We calculated velocity, movement, center entries, rearing and grooming events. Treatment with CNO significantly increased velocity, with a maximal 90% increase after 20 minutes of exploration in DS-DQ animals compared with wildtype and DS-VEH animals (Fig. 2, A and B). The DS-DQ rats showed a 65% increase in total movement over the course of 40 minutes (from 115.4 ± 17.4 m at baseline to 188.4 ± 46.7 m after treatment with CNO, $P<0.001$, n=12) (Fig. 2C), and total time moving increased by 49%. Wildtype rats had a 14% decrease in moving time following CNO treatment, which we attribute to a general habituation to the open field during the second exposure (Fig. 2E). Yet, the number of movement initiations (frequency) was similar in all groups (Fig. 2I). There was increased number of entries (+125%) and time spent (+119%) in the center of the open field in DS-DQ rats ($P<0.0001$, n=12) following CNO treatment (Fig. 2, F and J). Time spent rearing and number of rearing events were similarly increased with 66% and 99%, respectively ($P<0.001$, n=12) following CNO treatment in DS-DQ rats (Fig. 2, G and K). Grooming time and bouts were likewise affected, but in the opposite direction, with significant reductions of -59 and -38%, respectively ($P<0.001$, n=12) following CNO treatment (Fig. 2, H and L). Taken together, DS-DQ rats move and explore more following CNO treatment compared to WT and DS-VEH rats, while spending less time in self-grooming. Similarly, in the second batch of animals used for the imaging experiments, there was a 46% increase in total movement ($p=0.003$, n=9), an 82% increase in center entries ($p=0.005$, n=9), and a 43% increase in rearing events ($p=0.002$, n=9) in DS-DQ animals following CNO treatment in comparison to DS-VEH (Suppl. Fig. 4, A-C). There were no main effects of transfection or sex on either behavior.

*Nigro-striatal dopaminergic stimulation affects prepulse inhibition of the acoustic startle response differently in males and females*

We first tested the acoustic startle response (ASR) to different intensity sound pulses, as described in methods. The ASR was clearly measurable after exceeding 100 dB and plateaued at 110 dB both in males and females, with a maximal ASR (as measured at 120 dB) of 59.1 ± 8.1 % in males (n=21) and 49.6 ± 9.1 % in females (n=27) (Fig. 3A). Therefore, we chose 110 dB as the pulse intensity for subsequent testing of pre-pulse inhibition (PPI). There was a sex difference in the ASR to various volumes of sound pulses ($P<0.001$, $F(1,46)=25.2$), but no difference in the ASR between different transfections, either for male (Fig. 3B, $P=0.99$, $F(2,19)=0.009$) or female rats (Fig. 3C: $P=0.17$, $F(2,23)=1.937$). One female DS-DQ and one WT were excluded from the ASR analysis because of errors in the gain setting.

We next tested startle response (SR) to a 110 dB sound pulse with or without different intensity prepulses (all pulses are shown in Suppl. Fig. 5, A and D) and short-term habituation (STH) (Suppl. Fig. 5, B and E). There was no effect of transfections or treatment with CNO on the SR

(Fig. 3, D and E), but there was an overall effect of sex. SR was greater in males (58.1 ± 3.8 %, n=21) than in females (48.6 ± 4.3 %, n=27) (P<0.001, F(1,84)=30.64), as expected from the initial ASR test (Fig. 3A). There were no differences in STH between WT and transfection groups or between baseline and CNO treatment. However, the mean STH was significantly lower in males (-3.9 ± 7.7 %, n=21) than in females (19.7 ± 6.2 %; n=27) (Suppl. Fig. 5, B and E, P=0.008, F(1,86)=7.3).

In general, SRs decreased in proportion to the amplitude of the prepulse, as expected (Suppl. Fig. 5, A and D). There were no general effects of transfection or CNO treatment on SR in either sex. Yet, a reduced SR following CNO treatment in DS-DQ females was just shy of statistical significance (Ave. Diff. = 3.3 ± 1.5 %, p=0.0501 (F(1,9)=5.11)). The latency from startle pulse to startle onset and maximum peak of startle was assessed from the SR data above (Suppl. Fig. 5, C and F). There were no clear differences in latency, prepulse only and no stimuli (Suppl. Fig. 5H).

PPI following the 69 dB prepulse was higher in female (18.6 ± 5.3 %, n=27) than male rats (10.6 ± 4.4 %, n=21) (Suppl. Fig. 5G, p=0.006, F(1,84)=7.86) at baseline. Transfection did not affect baseline PPI in either sex (Fig. 3, F and G, and Suppl. Fig. 5G). There was a general 24% increase in DS-DQ female rats for all pre-pulses (p=0.022, F(1,9)=7.6), and an 58% increase in female DS-DQ rats at the 69 dB prepulse condition upon CNO treatment (p=0.018, n=10) (Fig. 3, G and I).

*Nigro-striatal dopaminergic stimulation affects metabolic functional connectivity between regions in the frontal cortex and striatum.*

The normalized whole brain uptake of [$^{18}$F]FDG at baseline in DS-DQ rats after CNO treatment showed a lower relative uptake in fronto-cortical and striatal regions, and higher relative uptake in hippocampal and cerebellar regions (Figure 4A). On a regional level, reductions in [$^{18}$F]FDG uptake were significant in the nucleus accumbens (NAc, P = 0.001, t = 4.08, DF = 49, N = 8) , DMS (P = 0.003, t = 3.80, DF = 49, N = 8) and medial prefrontal cortex (mPFC, P = 0.046, t = 2.83, DF = 49, N = 8) following CNO treatment in DS-DQ rats. There were no effects on [$^{18}$F]FDG uptake in DS-VEH rats (Fig. 4B) and no effects of sex or transfection.

Subsequently, we calculated correlations matrices for [$^{18}$F]FDG uptake in the CSTC circuit (Suppl. Fig. 6B) for the different conditions. The matrices were compared across conditions using a Fisher's Z-transformation and a permutation test. There was a significant effect on regional correlations following CNO treatment in the DS-DQ animals (P = 0.04), but no effect in DS-VEH animals (P = 0.68) or between transfections at baseline (P = 0.78) (Suppl. Fig. 6C). A *post hoc*, region-to-region correlation analysis was conducted to identify regional correlations within the CSTC circuit in DS-DQ animals (Fig. 4, D and E). The changes ($\Delta Z$) in correlations (Fig. 4F) revealed significant changes in the connectivity within the CSTC circuit (Fig. 4G). At

baseline in DS-DQ rats, there was a positive correlation between [$^{18}$F]FDG uptake in the orbitofrontal cortex (OFC) and the anterior cingulate cortex (ACC) (r = 0.85, Suppl. Fig. 7EE) and a negative correlation between the dorsolateral striatum (DLS) and both the OFC (r = -0.90, Suppl. Fig. 7F) and the ACC (r = -0.72, Suppl. Fig. 7J). The strength of these correlations decreased after CNO treatment (Suppl. Fig. 7, G, H and L).

*Nigro-striatal dopaminergic stimulation increase glutamate and N-acetylaspartate glutamate levels in medial prefrontal cortex and glutamate levels in dorsal striatum.*

Based on findings from normalized regional [$^{18}$F]FDG uptake (Fig. 4B), we chose two regions for MR spectroscopy (MRS) measurements *in vivo* of glutamate, glutamine, N-aspartate (NAA) and N-aspartateglutamate (NAAG). The mPFC had a voxel size of 2x3x3 mm$^3$ and DS a voxel size of 3x3x3 mm$^3$ (Fig. 5, A-C). A third region, NAc, with a voxel size of only 2x2x2 mm$^3$, proved to be too small to yield reliable MRS measurements. We have previously found no difference between baseline and CNO treatment in WT animals treated with 0.5 mg/kg CNO *(25)*. We found no effect of sex, in any group, neither of transfections at baseline. However, there were increases in glutamate ($P < 0.0001$, $t = 5.73$, $DF = 70$), total NAA+NAAG ($P = 0.006$, $t = 3.43$, $DF = 70$) and total glutamate + glutamine ($P = 0.001$, $t = 3.95$, $DF = 70$) levels in the mPFC following CNO treatment in DS-DQ rats (Fig. 5, D and E). Furthermore, increases in glutamate ($P < 0.0001$, $t = 5.67$, $DF = 70$) and total glutamate + glutamine ($P < 0.0001$, $t = 5.54$, $DF = 70$) levels were found in the DS. Contrary to our previous report *(25)*, CNO treatment in DS-VEH animals did provoke significant reductions in glutamate ($P = 0.0002$, $t = 4.69$, $DF = 70$) and total glutamate + glutamine ($P < 0.0001$, $t = 6.01$, $DF = 70$) levels (Fig. 6, F and G) in the DS.

## Discussion

We established a chemogenetic procedure for selective bilateral activation of nigro-striatal dopamine projections innervating the DMS, enabling us to test dopaminergic modulation of the CSTC circuit implicated in OCD and other disorders of the basal ganglia. The chemogenetic dopamine stimulation potentiated exploratory behavior, lowered self-grooming, and enhanced prepulse inhibition of the startle response, all of which are consistent with a shift away from an OCD-like behavioral phenotype. Multimodal molecular imaging studies with functional [$^{18}$F]FDG PET and MR spectroscopy revealed that dopamine release in DMS exerted a top-down modulatory control of cortical activity and the orchestration of behavior related to CSTC circuit function. These results in behaviorally normal rats are hypothesis-generating for a model that increased dopaminergic activity in DMS would reduce symptoms of OCD in animal models and patients.

*Nigro-striatal dopaminergic stimulation increases exploratory behaviors and lowers grooming*

We targeted subdivisions of striatal dopaminergic innervations by using of TH:CRE Long Evans Rats *(26)* treated with retrograde neuronal transfection by the AAV6 serotype, as previously established in rats *(27)*, mice *(28)* and non-human primates *(29)*. Activation of hM3Dq DREADDs induces phosphatidylinositol hydrolysis *(24)*, c-fos activation *(30–32)*, dopamine release *(11)* and increased neuronal excitability with a burst firing pattern *(31–34)*. *In vivo* hM3Dq DREADD stimulation of mesencephalic dopamine neurons induces persistent hyperlocomotion *(31, 35–39)*, as recapitulated in our findings in DS-DQ rats. We also observed an increase in exploratory behaviors, entries into center field, and rearing (supported and unsupported) in all DS-DQ rats following CHO-stimulation. Such exploratory behaviors typically increase following treatment with anxiolytic drugs *(40, 41)*, and decrease following stress *(41, 42)*, often in a manner independent of hyperlocomotion, thus suggesting anxiolytic effects of the present perturbation of the CSTC.

Grooming is an innate rodent behavior, characterized by a sequential pattern of movements *(43)*, and serves as a useful proxy for OCD-like compulsive behavior *(44)*. Grooming time and frequency are controlled by the efferent activity of striatal SPNs. Activation of $D_1$ receptors on SPNs of the direct ("go") pathway increase grooming, whereas activation of $D_2$ receptors on the indirect ("no-go") SPNs decrease grooming *(43)*. Our DS-DQ rats showed a significant decrease of grooming frequency and duration after dopaminergic DREADD stimulation. This may reflect preferential activation of the indirect pathway SPNs, although we cannot rule out the possibility of secondary effect due to hyperlocomotion and increased exploration. The preferential activation of the indirect pathway is supported by a recent report that the dopamine fibres innervating the DMS predominantly target $D_2$-positive SPNs *(45)*. Grooming is reported to follow an inverted U-shape function in response to stress *(46)*, yet we did not observe any changes in grooming or other stress induced behaviors such as rearing and entries into field center in WT or DS-VEH rats. Also, the startle response did not induce grooming in another study *(47)*, suggesting that there was no carryover of stress from the first testing session.

CNO metabolizes *in vivo* to clozapine, which is presumably the main agonist on DREADDs *(25, 48–50)*. Clozapine is an antagonist at endogenous dopamine $D_{2/3}$ and serotonin 5-$HT_{2A}$ receptors, but has selectivity for DREADDs when administered at the present low dose. Indeed, we did not observe any behavioral effects of CNO/clozapine in control rats in this study, nor had we seen any occupancy at $D_{2/3}$ or 5-$HT_{2A}$ receptors in an earlier *in vivo* binding experiment *(25)* at the dose used in these experiments, thus arguing for selective activation of DREADDs.

*Nigro-striatal dopaminergic stimulation affects prepulse inhibition of the acoustic startle response differently in males and females*

PPI is an autonomous behavioral response, which is highly modulated by components of the CSTC circuit, in particular the PFC *(51–54)*, striatum *(55)*, and the SN *(56)*. Disruption of normal PPI is evident in people with OCD *(57, 58)*. PPI and ASR are conserved across species and serve as translational constructs in brain research. While dopamine agonists disrupt PPI, the relative contributions of $D_1$-and $D_{2/3}$ receptor pathways are debated *(59–62)*. Thus, converging lines of clinical and preclinical evidence link the CSTC circuit, dopamine, and PPI. The expression of PPI differs between rodent strains *(63, 64)* and sex *(65–67)*. Indeed, we found in this study that DS-DQ stimulated female rats' had increased PPI at low prepulse amplitude, but males did not. Previous work showed that male rats with SN lesions *(56)* as well as male mice with striatal lesions *(68)* showed a disruption of PPI, but there was no investigation of female rats in these studies. In another study, deep brain stimulation (DBS) of the NAc disrupted PPI in control rats, whereas the same DBS rescued disrupted PPI in a rat model of schizophrenia *(53)*, which implies context-dependence of the behavior consequences of stimulated dopamine release. Clozapine can restore disrupted PPI *(61, 64, 69)*, but neither we nor others *(49)* have measured any intrinsic effects of CNO on PPI in wildtype or control animals at the dose used, thus linking dopamine activity in the DMS with expression of PPI especially in females.

*Nigro-striatal dopaminergic stimulation affects metabolic functional connectivity between regions in the frontal cortex and striatum.*

Metabolic mapping of [$^{18}$F]FDG uptake by PET can identify neuronal circuits related to behavior, chemical stimulation or chemogenetic-induced circuit modulation *(53, 54, 70–73)*. We evaluated the whole-brain normalized [$^{18}$F]FDG uptake in a fasting condition *(74)*. We found that DS-DQ stimulation elicited relative metabolic changes throughout the brain, with hypometabolism in frontal cortical and striatal areas, and hypermetabolism in cerebellum and thalamus (Fig 4A). In particular, three areas (mPFC, DMS and NAc, Fig 4B) within the CSTC circuit showed significant [$^{18}$F]FDG hypometabolism after DS-DQ stimulation. A *post-hoc* correlation analysis revealed disruption of the functional connectivity between pairs of regions, namely the Thal/mPFC, ACC/OFC, DLS/ACC, and DLS/OFC (Fig. 4G, S4 and S5), indicating reduced metabolic coherence between components of the CSTC circuit. Serveas et al. showed that acute treatment of rats with the dopamine $D_{2/3}$ receptor agonist quinpirole provoked a global increase in [$^{18}$F]FDG whole-brain uptake, yet a relatively lower increase in NAc, DS, and the frontal cortical regions, i.e. mPFC, ACC and OFC *(73)*, suggesting a common mechanism. Global increased [$^{18}$F]FDG uptake can hide regional differences in metabolism, emphasizing the importance of whole-brain normalization between baseline and condition *(75)*. Nordstrom et al. found that administration of another $D_2$ receptor agonist, bromocriptine suppressed "Tics" in a transgenic mouse model of Tourette's Syndrome *(76)*. Tourette's Syndrome and OCD have many common features, plausibly due to malfunctioning of the CSTC circuit in both conditions

*(77)*. Thus, the suppressive effects of bromocriptine on "Tics" are in-line with our observations, suggesting that agonism at MSNs expressing $D_2$ receptors stimulates the "indirect pathway" of the CSTC circuit. This may underlie the benefits derived from bromocriptine reported in patients with treatment-resistant OCD *(78)*. Thus, there is general agreement that various perturbations of the CSTC can have overlapping effects on metabolic connectivity. Our use of selective chemogenetic stimulation avoids possible confounding effects of dopamine agonism across the whole brain, presenting a more selective technique for dissecting regional functional connectivity.

*Nigro-striatal dopaminergic stimulation increases total glutamate levels in mPFC and DMS*

Changes in striatal dopamine and prefrontal cortical glutamate levels is part of the etiology of neuropsychiatric diseases which involve the CSTC circuit like OCD *(19)*. Our functional connectivity results with [$^{18}$F]FDG PET inspired us to investigate associated changes in glutamate levels. MR spectroscopy showed increase in glutamate and NAAG in the mPFC, and increased glutamate in the DMS.

In the mPFC, glutamate is stored in the terminals of glutamatergic afferents, which are presumably thalamic or cortical inputs to the mPFC, while NAAG is mainly located in interneurons *(79)*. Once released into the synapse, glutamate is taken up by astroglial cells and converted into glutamine, whereas NAAG is metabolized to NAA and glutamate *(80, 81)*. Increased glutamate and NAAG levels measured by MR spectroscopy may reflect elevated vesicular concentrations due to lower neuronal activity. NAAG signaling is not completely understood, but some evidence points towards an inhibitory effect on GABA release, such that lower NAAG release might result in net inhibition of corticostriatal projections *(82)*. This inhibition might thus account for the increased glutamate levels in DMS after DS-DQ stimulation. Furthermore, we suppose that DS-DQ stimulation also stimulate dopamine neurons that co-release glutamate *(83, 84)*, which in turn might favor the astroglial conversion of glutamine to glutamate *(80, 81)*. There is no general model to connect glutamate levels measured with MRS to [$^{18}$F]FDG uptake, and these two markers did no correlate in WT mice, although there was a clear inverse relationship in mGluR5 KO mice *(85)*. That finding resembles present findings in the DS-DQ group, suggesting a similar perturbation of the coupling between glutamate levels and energy metabolism.

*Translational relevance*

The associated reduction of OCD-like compulsive behavior (grooming) in our rats matches the reduction reported in the DB study. Changes in locomotor activity, grooming and sensory gating (PPI) are endophenotypes of OCD *(58, 86)*. Furthermore, meta-analysis of [$^{18}$F]FDG PET studies shows a fairly consistent pattern of frontal hypermetabolism and increased inter-regional correlation in OCD *(87)*. In a recent study with DBS of the NAc in people with OCD, striatal

dopamine release correlated with a decline in OCD related symptoms *(12)*. Similarly, our present activation of dopaminergic projections from SNpc to DMS elicited a relative hypometabolic state in OCD-associated regions within the CSTC circuit. Our results enable a disentanglement of the behavioral and metabolic effects of specific elements in the CSTC circuit and support the notion that dopamine activation could lower endophenotypes associated with OCD

*Conclusion*

Here we reported an effective and selective way to transfect dopamine neurons projecting from the SNpc to the DMS in the rat. This method could be adapted to other dopamine innervating regions like the DLS or NAc. Transfections with a Gq couple DREADD enabled selective activation of the nigro-striatal dopamine neurons and elicited a range of behavioral and neuronal responses related to the CSTC circuit and relief of symptoms in OCD. Nigro-striatal dopamine activation increased exploratory behaviors while also lowering grooming and enhanced the effects of pre-pulse inhibition. Furthermore, nigro-striatal dopamine activation elicited regional responses in the CSTC circuit as measured with [$^{18}$F]FDG PET and MR spectroscopy. A lower uptake in cortical and striatal areas was measured as a topdown response from nigro-striatal dopamine activation with a concurrent increase in total glutamate levels, believed to be a result of lower glutamatergic activity. A *post hoc* functional connectivity assessment showed that strong baseline connections in cortical and striatal function diminished after nigro-striatal dopamine activation. Taken together, nigro-striatal dopamine lowers behavioral and neuronal phenotypes associated with obsessive-compulsive disorder supporting findings with dopamine agonists and DBS in several preliminary clinical studies in people with OCD and providing a hypothesis; dopaminergic activity in DMS reduces symptoms of OCD in animal models and patients, for future studies.

## Materials and Methods

*Study Design*

In the first cohort (cohort 1) of animals, we confirmed the established targeted transfection model, with random assignment of rats to either the chemogenetic or the control group. We then tested the effects chemogenetic activation on open field locomotor behavior as well as CSTC-specific behavioral phenotypes, i.e. self-grooming and sensory gating. In the second cohort (cohort 2), we repeated the locomotor assessment and measured metabolic activity and functional connectivity in the CSTC circuit using [$^{18}$F]FDG PET, while also measuring local concentrations of energy metabolites with MRS. We excluded from consideration rats not showing bilateral expression of hM3Dq-DREADD to immunohistochemistry *post hoc*, along with statistically significant outliers in other experiments. We conclude by discussing the various results in the context of how altering dopamine transmission in the DMS may be relevant to the symptoms of OCD.

*Statistics*

Standard deviations (SD) are reported throughout the results and figures. Significance are reported as **** P<0.0001, *** P<0.001, ** P<0.01, * P<0.05. Specific statistical tests are described for each experiment below.

*Animals*

LE Tg(TH:Cre 3.1)Deis rats (TH:Cre rats) were purchased from the Rat Resource and Research Center (RRRC, University of Missouri). This strain carries a transgene in which Cre recombinase is inserted immediately before the start codon of the tyrosine hydroxylase gene (Th), which is expressed in the SNpc dopamine cells (Witten et al. 2011). In figures, we consistently depict data points from males using upwards pointing triangles (♂ = ▲) while data points from females are reported using downward pointing triangles (♀ =▼). Additional information of breeding and ethics is located in the supplementary materials.

*Retrograde chemogenetic transfection of dopaminergic projections in rats and mice*

Adult TH:Cre rats (250 g) rats were anesthetized with 3% isoflurane (vol/vol) in oxygen and placed into a stereotactic frame (Kopf Instruments, Tujunga, CA, USA) while on a water-heater at 40 ºC. Anesthesia was maintained with 1.5– 2% isoflurane; breathing, pain reflex, and body temperature was monitored throughout surgery. The scalp was shaved and disinfected with successive swabs soaked in 70% iodine, ethanol, and 0.1% lidocaine. An incision was then made down the midline of the scalp, the skull was exposed, and burr holes were drilled above the target regions. Portions of retrogradely transfecting viral vector (2 µL) were injected bilaterally at two locations in the DMS (AP +1.1 mm, ML ± 2.5 mm, DV -5 mm and -6 mm) via a 10 µl Nanofil syringe and 33GA beveled needle (World Precision Instruments, Sarasota, FL, USA) at an infusion rate of 150 nL/min. After the infusion, the needle was left in place for at least ten min to allow for diffusion of the virus away from the needle tip before its slow withdrawal. Vehicle animals received an injection with the control (hM3Dq-negative) virus. Following injections, the scalp was sutured and the rat was allowed to regain consciousness. Carprofen (5 mg/kg) was administered subcutaneously as an analgesic before surgery and at 24 and 48 h after surgery. Following surgery, rats were single-housed for one week, and their weight, fur, eyes and overall movement were checked daily for signs of distress following the scheme of Roughan and Flecknell *(88)*. Animals were then returned to group housing for two weeks prior to further experiments. Additional information on viral vectors is located in the supplementary materials.

*Immunohistochemistry*

Rats were euthanized with an overdose of pentobarbital (Glostrup Apotek, Denmark) and immediately perfused transcardially with 150-200 ml of ice-cold phosphate-buffered saline (PBS) followed by 100-150 ml of ice-cold 4% paraformaldehyde (PFA) in PBS. Brains were

removed and stored in 4% paraformaldehyde for 24 h at 4 °C, rinsed twice with PBS, and then cryoprotected in 30% sucrose/PBS. Brain sections 40 µm-thick obtained on a microtome were stored in cryoprotectant solution at -20 °C. Free-floating sections were immunostained for mCherry (Cat. #632543, TaKaRa Bio Europe) using the Avidin-Biotin Complex Peroxidase (ABC-P) method and for TH (Cat. #P21962, Invitrogen) using fluorescent antibodies. In the ABC-P method, slices were washed in 10 mM PBS, and then in 1% $H_2O_2$ in PBS. Non-specific binding was blocked with 5% normal sheep serum (NSS), 1% BSA, and 0.3% Triton X-100 (TX) in PBS. Sections were incubated at 4 ºC in primary antibody (1:1000 dilution in 1% BSA, 0.3% TX-100 in PBS) overnight and later washed in 0.1% TX in PBS followed by one hour incubation with secondary antibody at room temperature (1:1000 dilution in 1% BSA, 0.3% TX in PBS). After washing again, the samples were incubated another hour in ABC-P (Cat. #PK-6100, Vector laboratories) and rinsed in Tris-HCl before being developed in 0.1% diaminobenzidine (DAB). In the fluorescent method, nonspecific binding was blocked with 0.2% BSA, 0.2% TX, and normal donkey serum (NDS) in PBS at room temperature, before incubation with primary antibody (diluted 1:500 in PBS) overnight at 4 ºC. Sections were then washed and blocked with 2% NDS before a 2-hour incubation in fluorescent secondary antibody (1:200 in PBS) at room temperature in dark. Stained sections were mounted on slides, covered with Pertex or antifade mounting medium, and imaged with a Zeiss Axio Imager Z.1 imager microscope. Digital images of ABC-P stained brain slices were analyzed to assemble a depiction of the extent and pattern of transfection in the target regions.

*Locomotor activity*

The spontaneous locomotor activity was recorded from 43 animals in cohort 1 at baseline and after CNO treatment (14 WT (7M / 7F), 15 DS-DQ (8M / 7F) and 14 DS-VEH rats (7M / 7F)) in a custom-made open field maze consisting of an 80 x 80 cm arena enclosed by 65 cm opaque walls, with indirect, dim illumination (~10 Lux). On the test day, DREADD or control rats received an i.p. injection of CNO (0.5 mg/kg in 5% DMSO/Saline), and 20 min later were placed at the center of the open field and allowed to explore for 40 minutes. Behavior was recorded with a Basler ace2 Pro video camera with a 4.5-12.5 mm F1.2 lens positioned directly above the arena and analyzed using ethovision software, with scoring of distance travelled, velocity, center of field entries, rearing and grooming. The arena was cleaned with soap and water and then dried between each session.

*Acoustic startle response*

Startle tests were conducted in a sound-attenuated, lighted and ventilated chamber (StartFear Combined system, Panlab Harvard Apparatus, Barcelona, Spain). The chamber (67 x 53 x 55 cm) contains a behavioral box (25 x 25 x 25 cm) mounted on a load cell platform, a loudspeaker mounted above the animal, and a small LED light for illumination during testing. Animals were held in a Plexiglas cylinder (225 mm length x 74 mm diameter) mounted on a grid floor by

plastic screws. Startle responses were detected using weight transducers placed under each leg of the load cell platform, and the response was amplified and digitized over a range of 0–100 arbitrary units. The amplitude of the startle response is defined as the largest peak value within 1 s after the onset of the startle stimulus. Data collection and sequencing of all stimuli are controlled by the supplied hardware and software (Packwin V2.0).

The startle response of the rats was assessed before the PPI tests. After an exploration period of 10 min with a constant background white noise of 65 dB for acclimation, 55 startle stimuli of 20 ms duration. (70-120 dB white noise (w.n.), in 5 dB intervals, 5 of each) were presented in a pseudo-randomized order, with variable pseudo-randomized inter-trial intervals (ITI; range 6-24s, mean 15 s) to avoid predictability of the next stimulation. The startle response corresponding to each pulse was plotted for each rat and the maximum pulse intensity was established.

*Prepulse inhibition of the acoustic startle response*

Immediately after the locomotion recordings, the rats were transferred to the startle chamber for sensorimotor gating assessment. The session consisted of four blocks. Block I was a 5 min exploration period with only background noise (65 dB w.n.). Block II was a short-term habituation (STH) test with 10 pulses (110 dB w.n., 30 ms each at ITI of 10 s). Block III was the proper startle and pre-pulse inhibition (PPI) test, consisting of seven different trials; a) no stimuli (65 dB background noise); b) pulse alone (110 dB w.n., 30 ms); c) pre-pulse alone (81 dB w.n., 20 ms); d-g) pulse (110 dB w.n., 30 ms) preceded 100 ms by a 20 ms w.n. pre-pulse at 69 dB (d), 73 dB (e), 77 dB (f) or 81 dB (g). Each trial type was presented 15 times in a pseudo-randomized order with a variable ITI ranging from 6-24 s (15 s mean). Block IV was another STH test, conducted just as Block II. The percentage of PPI for each pre-pulse intensity was expressed as: % PPI = [(mean startle amplitude on pulse alone trial – mean startle amplitude on pre-pulse trial)/mean startle amplitude on pulse alone trial] *100.

*[$^{18}$F]FDG PET scanning*

The rats were fasted overnight and brought to the scanning room at least two hours before the scan. Here they received an s.c. injection of 0.5 mg/kg CNO (n=14, (7 DS-DQ, 4F/3M), (7 DS-VEH, 4F/3M)) or saline followed 20 min later by an i.p. injection of 14.1 ± 1.6 MBq FDG (from the clinical in-house production of The Department of Clinical Physiology, Nuclear Medicine and PET, Righospitalet, Denmark, where the PET scans were also conducted). The rats remained in their home cage for 45 minutes following the [$^{18}$F]FDG injection. Following this uptake period, the rats were sedated with isoflurane (2–2.5% in oxygen) and rapidly placed in a homemade four rat insert at the center of the aperture of a Siemens HRRT (High Resolution Research Tomograph) scanner *(89)* for a 45-min list-mode emission scan followed by a rotating point source $^{137}$Cs transmission scan *(90)*. The rats were kept warm using an infrared lamp and

monitored for respiration throughout the scan. The list-mode emission data were dynamically reconstructed with the standard 3D-OP-OSEM-algorithm and corrected for attenuation and scatter algorithm using point-spread function modelling (PSF) *(90)*. Each image was adjusted for body weight and injected dose (Standardized Uptake Value, SUV). PET images were cropped to brain only images for each rat in PMOD and an automatic co-registration to an-FDG-specific rat brain template using FLIRT in FSL (cross correlation cost function with 12 degrees of freedom) *(91)*. Each individual scan was normalized using a whole-brain normalization factor (NF = Average whole-brain uptake/individual whole-brain uptake). A VOI-atlas (PMOD) with select regions from the CSTC circuit was used for VOI-extraction. The seven ROIs/VOIs were: nucleus accumbens (NAc), dorsomedial striatum (DMS), dorsolateral striatum (DLS), anterior cingulate cortex (ACC), medial prefrontal cortex (mPFC), orbital frontal cortex (oFC) and thalamus (Thal).

*Image analysis*

The images were averaged per group/condition and the difference, higher or lower uptake in CNO condition compared with baseline, was calculated within each group (DS-DQ and DS-VEH) in PMOD. A regional analysis within the CSTC circuit (NAc, ACC, DMS, DLS, oFC, mPFC, Thalamus) was done for each animal. The mean difference in FDG uptake between conditions (baseline & CNO) in the two groups (DS-DQ, DS-VEH) was calculated in Prism using mixed-effects model with Sidak's multiple comparisons test. Next, we evaluated condition and group differences in FDG correlation between regions in the CSTC circuit (Fig. S4). For a specific group/condition, a Pearson's correlation coefficient was calculated between each region pair and transformed using Fisher's r-to-z transformation, to allow for comparison of data with heterogeneous distributions *(92)*. All Fisher's z-transformed correlations for each group (DS-DQ, DS-VEH) in either baseline or CNO condition were assembled, yielding four matrices: DS-DQ (baseline), DS-DQ (CNO), DS-VEH (baseline), DS-VEH (CNO) (Figure S4C). Circuit-wide FDG correlations for each condition/group were estimated as the sum of the absolute value of z-transformed values across all unique region pairs (i.e., lower or upper triangles of the correlation matrix). Permutation testing (10,000 permutations) was used to derive an empirical null distribution and estimate statistical significance. For each permutation, respective condition/group status was scrambled prior to computing the CSTC circuit correlation matrix and sum of absolute z-transformed values. Condition/group differences were considered statistically significant if the permutation derived p-value was less than 0.05. Subsequently, a *post hoc* test in DS-DQ animals was performed for each region-to-region correlation. For each region pair, a null distribution was derived by scrambling regional FDG values with respect to each other and estimating the correlation. Observed p-values for the *post hoc* analysis were family-wise error-corrected across all the region-to-region pairs using Bonferroni-Holm *(93)*.

*Magnetic resonance spectroscopy*

All MR scans were performed on a Bruker BioSpec 94/30 USR MRI system (9.4T, 30 cm bore, Bruker, Ettlingen, Germany) at the University of Copenhagen using a quadrature rat brain surface coil and an 86 mm rat body volume coil (and Paravision 5.3 acquisition software) (Bruker Ettlingen, Germany) as previously described (29). Rats were anaesthetized with 2% isoflurane in oxygen and placed in the scanner. The magnetic field was adjusted to obtain global and local homogeneity. MRI was performed using a TurboRARE sequence, MRS was done sequentially in a 3 x 3 x 3 mm region in the right hemispheric DS and then in a 3 x 2 x 3 mm region in mPFC (about 20 min. for each region). The spectra's was acquired using a STEAM sequence with TE = 4 ms, TR = 4000 ms, 400 averages, eight dummy scans and 4096 points. VAPOR was used for water suppression. Metabolite concentration calculation was performed by LCModel using water unsuppressed signal as an internal reference.

**References**

1. A. M. Graybiel, Chapter 10 - The Basal Ganglia, *Conn's Transl. Neurosci.* , 219–225 (2017).
2. S. E. Ahmari, D. D. Dougherty, DISSECTING OCD CIRCUITS: FROM ANIMAL MODELS TO TARGETED TREATMENTS, *Depress. Anxiety* **32**, 550–562 (2015).
3. J. H. Lee, R. Durand, V. Gradinaru, F. Zhang, I. Goshen, D.-S. Kim, L. E. Fenno, C. Ramakrishnan, K. Deisseroth, Global and local fMRI signals driven by neurons defined optogenetically by type and wiring., *Nature* **465**, 788–92 (2010).
4. E. Garr, A. R. Delamater, Chemogenetic inhibition in the dorsal striatum reveals regional specificity of direct and indirect pathway control of action sequencing, *Neurobiol. Learn. Mem.* **169**, 107169 (2020).
5. L. Polyanska, H. D. Critchley, C. L. Rae, Centrality of prefrontal and motor preparation cortices to Tourette Syndrome revealed by meta-analysis of task-based neuroimaging studies, *NeuroImage Clin.* **16**, 257–267 (2017).
6. E. H. Simpson, C. Kellendonk, Insights About Striatal Circuit Function and Schizophrenia From a Mouse Model of Dopamine D2 Receptor Upregulation, *Biol. Psychiatry* **81**, 21–30 (2017).
7. S. E. Ahmari, T. Spellman, N. L. Douglass, M. A. Kheirbek, H. B. Simpson, K. Deisseroth, J. A. Gordon, R. Hen, Repeated cortico-striatal stimulation generates persistent OCD-like behavior., *Science* **340**, 1234–9 (2013).
8. H. Edemann-Callesen, B. Habelt, F. Wieske, M. Jackson, N. Khadka, D. Mattei, N. Bernhardt, A. Heinz, D. Liebetanz, M. Bikson, F. Padberg, R. Hadar, M. A. Nitsche, C. Winter, Non-invasive modulation reduces repetitive behavior in a rat model through the sensorimotor cortico-striatal circuit, *Transl. Psychiatry* **8** (2018), doi:10.1038/s41398-017-0059-5.
9. E. Nespoli, F. Rizzo, T. Boeckers, U. Schulze, B. Hengerer, Altered dopaminergic regulation of the dorsal striatum is able to induce tic-like movements in juvenile rats, *PLoS One* **13**, 1–23 (2018).
10. L. Y. Duan, N. K. Horst, S. A. W. Cranmore, N. Horiguchi, R. N. Cardinal, Controlling one ' s world : identification of sub-regions of primate PFC underlying goal-directed behavior, *bioRxiv* **11**, 1–37 (2021).
11. K. Mimura, Y. Nagai, K. Inoue, J. Matsumoto, Y. Hori, C. Sato, K. Kimura, T. Okauchi, T.

Hirabayashi, H. Nishijo, N. Yahata, M. Takada, T. Suhara, M. Higuchi, T. Minamimoto, Chemogenetic activation of nigrostriatal dopamine neurons in freely moving common marmosets, , 1–10 (2021).
12. M. Figee, J. Luigjes, R. Smolders, C. E. Valencia-Alfonso, G. Van Wingen, B. De Kwaasteniet, M. Mantione, P. Ooms, P. De Koning, N. Vulink, N. Levar, L. Droge, P. Van Den Munckhof, P. Richard Schuurman, A. Nederveen, W. Van Den Brink, A. Mazaheri, M. Vink, D. Denys, Deep brain stimulation restores frontostriatal network activity in obsessive-compulsive disorder, *Nat. Neurosci.* **16**, 386–387 (2013).
13. C. Zuo, Y. Ma, B. Sun, S. Peng, H. Zhang, D. Eidelberg, Y. Guan, Metabolic Imaging of Bilateral Anterior Capsulotomy in Refractory Obsessive Compulsive Disorder: an FDG PET Study, *J. Cereb. Blood Flow Metab.* **33**, 880–887 (2013).
14. B. Horwitz, S. E. Swedo, C. L. Grady, P. Pietrini, M. B. Schapiro, J. L. Rapoport, S. I. Rapoport, Cerebral metabolic pattern in obsessive-compulsive disorder: Altered intercorrelations between regional rates of glucose utilization, *Psychiatry Res. Neuroimaging* **40**, 221–237 (1991).
15. L. Menzies, S. R. Chamberlain, A. R. Laird, S. M. Thelen, B. J. Sahakian, E. T. Bullmore, Integrating evidence from neuroimaging and neuropsychological studies of obsessive-compulsive disorder: The orbitofronto-striatal model revisited, *Neurosci. Biobehav. Rev.* **32**, 525–549 (2008).
16. S. P. Whiteside, J. D. Port, J. S. Abramowitz, A meta–analysis of functional neuroimaging in obsessive–compulsive disorder, *Psychiatry Res. Neuroimaging* **132**, 69–79 (2004).
17. S. N. Haber, Corticostriatal circuitry, *Dialogues Clin. Neurosci.* **18**, 7–21 (2016).
18. Y. Aoki, A. Aoki, H. Suwa, Reduction of N-acetylaspartate in the medial prefrontal cortex correlated with symptom severity in obsessive-compulsive disorder: Meta-analyses of 1 H-MRS studies, *Transl. Psychiatry* **2**, e153-10 (2012).
19. D. R. Rosenberg, F. P. Macmaster, M. S. Keshavan, K. D. Fitzgerald, C. M. Stewart, G. J. Moore, Decrease in caudate glutamatergic concentrations in pediatric obsessive-compulsive disorder patients taking paroxetine, *J. Am. Acad. Child Adolesc. Psychiatry* **39**, 1096–1103 (2000).
20. D. R. Rosenberg, Y. Mirza, A. Russell, J. Tang, J. M. Smith, S. P. Banerjee, R. Bhandari, M. Rose, J. Ivey, C. Boyd, G. J. Moore, Reduced anterior cingulate glutamatergic concentrations in childhood OCD and major depression versus healthy controls, *J. Am. Acad. Child Adolesc. Psychiatry* **43**, 1146–1153 (2004).
21. M. Palner, C. Kjaerby, G. M. Knudsen, P. Cumming, Effects of unilateral 6-OHDA lesions on [ 3H]-N- propylnorapomorphine binding in striatum ex vivo and vulnerability to amphetamine-evoked dopamine release in rat, *Neurochem. Int.* **58**, 243–247 (2011).
22. C. Casteels, E. Lauwers, G. Bormans, V. Baekelandt, K. Van Laere, Metabolic-dopaminergic mapping of the 6-hydroxydopamine rat model for Parkinson's disease., *Eur. J. Nucl. Med. Mol. Imaging* **35**, 124–34 (2008).
23. J. Sala-Bayo, L. Fiddian, S. R. O. Nilsson, M. E. Hervig, C. McKenzie, A. Mareschi, M. Boulos, P. Zhukovsky, J. Nicholson, J. W. Dalley, J. Alsiö, T. W. Robbins, Dorsal and ventral striatal dopamine D1 and D2 receptors differentially modulate distinct phases of serial visual reversal learning, *Neuropsychopharmacology* **45**, 736–744 (2020).
24. B. N. Armbruster, X. Li, M. H. Pausch, S. Herlitze, B. L. Roth, Evolving the lock to fit the key to create a family of G protein-coupled receptors potently activated by an inert ligand., *Proc. Natl. Acad. Sci. U. S. A.* **104**, 5163–8 (2007).
25. S. Baerentzen, A. Casado-Sainz, D. Lange, V. Shalgunov, I. M. Tejada, M. Xiong, E. T.

L'Estrade, F. G. Edgar, H. Lee, M. M. Herth, M. Palner, S. Bærentzen, A. Casado-Sainz, D. Lange, V. Shalgunov, I. M. Tejada, M. Xiong, E. T. L'Estrade, F. G. Edgar, H. Lee, M. M. Herth, M. Palner, The chemogenetic receptor ligand Clozapine N-oxide induces in vivo neuroreceptor occupancy and reduces striatal glutamate levels, *Front. Neurosci.* **13**, 187 (2019).
26. I. B. B. Witten, E. E. E. Steinberg, S. Y. Y. Lee, T. J. J. Davidson, K. A. A. Zalocusky, M. Brodsky, O. Yizhar, S. L. L. Cho, S. Gong, C. Ramakrishnan, G. D. D. Stuber, K. M. M. Tye, P. H. H. Janak, K. Deisseroth, Recombinase-Driver Rat Lines: Tools, Techniques, and Optogenetic Application to Dopamine-Mediated Reinforcement, *Neuron* **72**, 721–733 (2011).
27. E. A. Salegio, L. Samaranch, A. P. Kells, G. Mittermeyer, W. San Sebastian, S. Zhou, J. Beyer, J. Forsayeth, K. S. Bankiewicz, Axonal transport of adeno-associated viral vectors is serotype-dependent, *Gene Ther.* **20**, 348–352 (2013).
28. D. F. Aschauer, S. Kreuz, S. Rumpel, Analysis of Transduction Efficiency, Tropism and Axonal Transport of AAV Serotypes 1, 2, 5, 6, 8 and 9 in the Mouse Brain, *PLoS One* **8**, e76310 (2013).
29. W. San Sebastian, L. Samaranch, G. Heller, a P. Kells, J. Bringas, P. Pivirotto, J. Forsayeth, K. S. Bankiewicz, Adeno-associated virus type 6 is retrogradely transported in the non-human primate brain., *Gene Ther.* **20**, 1178–83 (2013).
30. J. O. Szablowski, A. Lee-gosselin, B. Lue, D. Malounda, M. G. Shapiro, Non-Invasive Control of Neural Circuits, *Nat. Biomed. Eng.* **2**, 1–11 (2018).
31. S. V. Mahler, Z. D. Brodnik, B. M. Cox, W. C. Buchta, B. S. Bentzley, Z. A. Cope, E. C. Lin, M. D. Riedy, M. D. Scofield, J. Messinger, A. C. Riegel, R. A. España, G. Aston-Jones, Chemogenetic Manipulations of Ventral Tegmental Area Dopamine Neurons Reveal Multifaceted Roles in Cocaine Abuse, *bioRxiv* **39**, 503–518 (2018).
32. J. Cho, S. Ryu, S. Lee, J. Kim, H. I. Kim, Optimizing clozapine for chemogenetic neuromodulation of somatosensory cortex, *Sci. Rep.* **10**, 1–11 (2020).
33. N. R. Sciolino, N. W. Plummer, Y.-W. Chen, G. M. Alexander, S. D. Robertson, S. M. Dudek, Z. A. McElligott, P. Jensen, Recombinase-Dependent Mouse Lines for Chemogenetic Activation of Genetically Defined Cell Types, *Cell Rep.* **15**, 2563–2573 (2016).
34. M. T. Dell'Anno, M. Caiazzo, D. Leo, E. Dvoretskova, L. Medrihan, G. Colasante, S. Giannelli, I. Theka, G. Russo, L. Mus, G. Pezzoli, R. R. Gainetdinov, F. Benfenati, S. Taverna, A. Dityatev, V. Broccoli, Remote control of induced dopaminergic neurons in parkinsonian rats, *J. Clin. Invest.* **124**, 3215–3229 (2014).
35. J. Bonaventura, M. A. G. Eldridge, F. Hu, J. L. Gomez, M. Sanchez-Soto, A. M. Abramyan, S. Lam, M. A. Boehm, C. Ruiz, M. R. Farrell, A. Moreno, I. M. Galal Faress, N. Andersen, J. Y. Lin, R. Moaddel, P. J. Morris, L. Shi, D. R. Sibley, S. V. Mahler, S. Nabavi, M. G. Pomper, A. Bonci, A. G. Horti, B. J. Richmond, M. Michaelides, High-potency ligands for DREADD imaging and activation in rodents and monkeys, *Nat. Commun.* **10** (2019), doi:10.1038/s41467-019-12236-z.
36. A. H. Runegaard, C. M. Fitzpatrick, D. P. D. Woldbye, J. T. Andreasen, A. T. Sørensen, U. Gether, Modulating Dopamine Signaling and Behavior with Chemogenetics: Concepts, Progress, and Challenges, *Pharmacol. Rev.* **71**, 123–156 (2019).
37. B. P. Jackson, S. M. Dietz, R. M. Wightman, Fast-Scan Cyclic Voltammetry of 5-Hydroxytryptamine, *Anal. Chem.* **67**, 1115–1120 (1995).
38. S. Wang, Y. Tan, J. E. Zhang, M. Luo, Pharmacogenetic activation of midbrain dopaminergic neurons induces hyperactivity, *Neurosci. Bull.* **29**, 517–524 (2013).
39. A. J. Boender, J. W. de Jong, L. Boekhoudt, M. C. M. Luijendijk, G. van der Plasse, R. a H.

Adan, Combined use of the canine adenovirus-2 and DREADD-technology to activate specific neural pathways in vivo., *PLoS One* **9**, e95392 (2014).
40. L. Prut, C. Belzung, The open field as a paradigm to measure the effects of drugs on anxiety-like behaviors: A review, *Eur. J. Pharmacol.* **463**, 3–33 (2003).
41. M. Carli, C. Prontera, R. Samanin, Effect of 5-HT1A agonists on stress-induced deficit in open field locomotor activity of rats: Evidence that this model identifies anxiolytic-like activity, *Neuropharmacology* **28**, 471–476 (1989).
42. O. Sturman, P. L. Germain, J. Bohacek, Exploratory rearing: a context- and stress-sensitive behavior recorded in the open-field test, *Stress* **21**, 443–452 (2018).
43. K. C. Berridge, J. W. Aldridge, Super-stereotypy I: Enhancement of a complex movement sequence by systemic dopamine D1 agonists, *Synapse* **37**, 194–204 (2000).
44. A. V Kalueff, A. M. Stewart, C. Song, K. C. Berridge, A. M. Graybiel, J. C. Fentress, Neurobiology of rodent self-grooming and its value for translational neuroscience, *Nat. Rev. Neurosci.* **17**, 45–59 (2016).
45. J. Lu, Y. Cheng, X. Xie, K. Woodson, J. Bonifacio, E. Disney, B. Barbee, X. Wang, M. Zaidi, J. Wang, Whole-Brain Mapping of Direct Inputs to Dopamine D1 and D2 Receptor-Expressing Medium Spiny Neurons in the Posterior Dorsomedial Striatum, *eneuro* , ENEURO.0348-20.2020 (2020).
46. A. Fernández-Teruel, C. Estanislau, Meanings of self-grooming depend on an inverted U-shaped function with aversiveness, *Nat. Rev. Neurosci.* **17**, 591 (2016).
47. M. Xu, L. Li, C. Pittenger, Ablation of fast-spiking interneurons in the dorsal striatum, recapitulating abnormalities seen post-mortem in Tourette syndrome, produces anxiety and elevated grooming, *Neuroscience* **324**, 321–329 (2016).
48. A.-K. Ilg, T. Enkel, D. Bartsch, F. Bähner, Behavioral Effects of Acute Systemic Low-Dose Clozapine in Wild-Type Rats: Implications for the Use of DREADDs in Behavioral Neuroscience, *Front. Behav. Neurosci.* **12** (2018), doi:10.3389/fnbeh.2018.00173.
49. D. A. A. MacLaren, R. W. Browne, J. K. Shaw, S. Krishnan Radhakrishnan, P. Khare, R. A. Espana, S. D. Clark, Clozapine N-Oxide Administration Produces Behavioral Effects in Long-Evans Rats: Implications for Designing DREADD Experiments, *eNeuro* **3**, 219–16 (2016).
50. J. L. Gomez, J. Bonaventura, W. Lesniak, W. B. Mathews, P. Sysa-shah, L. A. Rodriguez, R. J. Ellis, C. T. Richie, B. K. Harvey, R. F. Dannals, M. G. Pomper, A. Bonci, M. Michaelides, Chemogenetics Revealed: Dreadd Occupancy and Activation Via Converted Clozapine, *Science (80-. ).* **357**, 503–507 (2017).
51. M. Bubser, M. Koch, Prepulse inhibition of the acoustic startle response of rats is reduced by 6-hydroxydopamine lesions of the medial prefrontal cortex., *Psychopharmacology (Berl).* **113**, 487–92 (1994).
52. K. Zavitsanou, Dopamine Antagonists in the Orbital Prefrontal Cortex Reduce Prepulse Inhibition of the Acoustic Startle Reflex in the Rat, *Pharmacol. Biochem. Behav.* **63**, 55–61 (1999).
53. L. Bikovsky, R. Hadar, M. L. Soto-Montenegro, J. Klein, I. Weiner, M. Desco, J. Pascau, C. Winter, C. Hamani, Deep brain stimulation improves behavior and modulates neural circuits in a rodent model of schizophrenia, *Exp. Neurol.* **283**, 142–150 (2016).
54. C. Rohleder, D. Wiedermann, B. Neumaier, A. Drzezga, L. Timmermann, R. Graf, F. M. Leweke, H. Endepols, The Functional Networks of Prepulse Inhibition: Neuronal Connectivity Analysis Based on FDG-PET in Awake and Unrestrained Rats, *Front. Behav. Neurosci.* **10**, 148 (2016).

55. N. R. Swerdlow, M. A. Geyer, D. L. Braff, Neural circuit regulation of prepulse inhibition of startle in the rat: Current knowledge and future challenges, *Psychopharmacology (Berl).* **156**, 194–215 (2001).
56. M. Koch, M. Fendt, B. D. Kretschmer, Role of the substantia nigra pars reticulata in sensorimotor gating, measured by prepulse inhibition of startle in rats, *Behav. Brain Res.* **117**, 153–162 (2000).
57. S. E. Ahmari, V. B. Risbrough, M. A. Geyer, H. B. Simpson, Prepulse Inhibition Deficits in Obsessive-Compulsive Disorder are More Pronounced in Females, *Neuropsychopharmacology* **41**, 2963–2964 (2016).
58. S. E. Ahmari, V. B. Risbrough, M. A. Geyer, H. B. Simpson, Impaired sensorimotor gating in unmedicated adults with obsessive-compulsive disorder, *Neuropsychopharmacology* **37**, 1216–1223 (2012).
59. S. Rodrigues, C. Salum, T. L. Ferreira, Dorsal striatum D1-expressing neurons are involved with sensorimotor gating on prepulse inhibition test, *J. Psychopharmacol.* , 026988111668687 (2017).
60. M. Bortolato, G. N. Aru, M. Fà, R. Frau, M. Orrù, P. Salis, A. Casti, G. C. Luckey, G. Mereu, G. L. Gessa, Activation of D1, but not D2 receptors potentiates dizocilpine-mediated disruption of prepulse inhibition of the startle, *Neuropsychopharmacology* **30**, 561–574 (2005).
61. M. A. Geyer, K. Krebs-Thomson, D. L. Braff, N. R. Swerdlow, *Pharmacological studies of prepulse inhibition models of sensorimotor gating deficits in schizophrenia: A decade in review* (2001).
62. M. Weber, W.-L. Chang, M. R. Breier, A. Yang, M. J. Millan, N. R. Swerdlow, The effects of the dopamine D2 agonist sumanirole on prepulse inhibition in rats, *Eur. Neuropsychopharmacol.* **20**, 421–425 (2010).
63. C. F. Plappert, P. K. D. Pilz, H.-U. Schnitzler, Factors governing prepulse inhibition and prepulse facilitation of the acoustic startle response in mice., *Behav. Brain Res.* **152**, 403–412 (2004).
64. N. Swerdlow, M.D., Ph.D., Discrepant Findings of Clozapine Effects on Prepulse Inhibition of Startle: Is It the Route or the Rat?, *Neuropsychopharmacology* **18**, 50–56 (1998).
65. M. M. Faraday, Rat sex and strain differences in responses to stress, *Physiol. Behav.* **75**, 507–522 (2002).
66. J. Lehmann, C. R. Pryce, J. Feldon, Sex differences in the acoustic startle response and prepulse inhibition in Wistar rats, *Behav. Brain Res.* **104**, 113–117 (1999).
67. F. Tylš, T. Páleníček, L. Kadeřábek, M. Lipski, A. Kubešová, J. Horáček, Sex differences and serotonergic mechanisms in the behavioural effects of psilocin, *Behav. Pharmacol.* **27**, 309–320 (2016).
68. L. C. Baldan Ramsey, M. Xu, N. Wood, C. Pittenger, Lesions of the dorsomedial striatum disrupt prepulse inhibition, *Neuroscience* **180**, 222–228 (2011).
69. L. De Carolis, M. A. Stasi, O. Serlupi-Crescenzi, F. Borsini, P. Nencini, The effects of clozapine on quinpirole-induced non-regulatory drinking and prepulse inhibition disruption in rats, *Psychopharmacology (Berl).* **212**, 105–115 (2010).
70. N. Apetz, E. Kordys, M. Simon, B. Mang, M. Aswendt, D. Wiedermann, B. Neumaier, A. Drzezga, L. Timmermann, H. Endepols, Effects of subthalamic deep brain stimulation on striatal metabolic connectivity in a rat hemiparkinsonian model, *DMM Dis. Model. Mech.* **12** (2019), doi:10.1242/dmm.039065.
71. D. J. Urban, H. Zhu, C. A. Marcinkiewcz, M. Michaelides, H. Oshibuchi, D. Rhea, D. K.

Aryal, M. S. Farrell, E. Lowery-Gionta, R. H. J. Olsen, W. C. Wetsel, T. L. Kash, Y. L. Hurd, L. H. Tecott, B. L. Roth, Elucidation of The Behavioral Program and Neuronal Network Encoded by Dorsal Raphe Serotonergic Neurons., *Neuropsychopharmacology* , 1–12 (2015).
72. M. Michaelides, S. A. R. Anderson, M. Ananth, D. Smirnov, P. K. Thanos, J. F. Neumaier, G. Wang, N. D. Volkow, Y. L. Hurd, Technical advance Whole-brain circuit dissection in free-moving animals reveals cell-specific mesocorticolimbic networks, **123** (2013), doi:10.1172/JCI72117.5342.
73. S. Servaes, D. Glorie, J. Verhaeghe, L. Wyffels, S. Stroobants, S. Staelens, [18F]-FDG PET neuroimaging in rats with quinpirole-induced checking behavior as a model for obsessive compulsive disorder, *Psychiatry Res. Neuroimaging* **257**, 31–38 (2016).
74. S. Deleye, J. Verhaeghe, L. wyffels, S. Dedeurwaerdere, S. Stroobants, S. Staelens, Towards a reproducible protocol for repetitive and semi-quantitative rat brain imaging with 18 F-FDG: Exemplified in a memantine pharmacological challenge, *Neuroimage* **96**, 276–287 (2014).
75. P. Borghammer, P. Cumming, J. Aanerud, A. Gjedde, Artefactual subcortical hyperperfusion in PET studies normalized to global mean: Lessons from Parkinson's disease, *Neuroimage* **45**, 249–257 (2009).
76. E. J. Nordstrom, K. C. Bittner, M. J. McGrath, C. R. Parks, F. H. Burton, Hyperglutamatergic cortico-striato-thalamo-cortical circuit breaker drugs alleviate tics in a transgenic circuit model of Tourette's syndrome, *Brain Res.* **1629**, 38–53 (2015).
77. Z. Wang, T. V Maia, R. Marsh, T. Colibazzi, A. Gerber, B. S. Peterson, The neural circuits that generate tics in Tourette's syndrome., *Am. J. Psychiatry* **168**, 1326–37 (2011).
78. A. Ceccherini-Nelli, M. Guazzelli, Treatment of refractory OCD with the dopamine agonist bromocriptine., *J. Clin. Psychiatry* **55**, 415–6 (1994).
79. J. R. Moffett, M. A. A. Namboodiri, J. H. Neale, Enhanced carbodiimide fixation for immunohistochemistry: Application to the comparative distributions of N-acetylaspartylglutamate and N- acetylaspartate immunoreactivities in rat brain, *J. Histochem. Cytochem.* **41**, 559–570 (1993).
80. L. K. Bak, A. Schousboe, H. S. Waagepetersen, The glutamate/GABA-glutamine cycle: aspects of transport, neurotransmitter homeostasis and ammonia transfer., *J. Neurochem.* **98**, 641–53 (2006).
81. N. Agarwal, P. F. Renshaw, Proton MR spectroscopy - Detectable major neurotransmitters of the brain: Biology and possible clinical applications, *Am. J. Neuroradiol.* **33**, 595–602 (2012).
82. J. Zhao, E. Ramadan, M. Cappiello, B. Wroblewska, T. Bzdega, J. H. Neale, NAAG inhibits KCl-induced [3H]-GABA release via mGluR3, cAMP, PKA and L-type calcium conductance, *Eur. J. Neurosci.* **13**, 340–346 (2001).
83. D. Sulzer, M. P. Joyce, L. Lin, D. Geldwert, S. N. Haber, T. Hattori, S. Rayport, Dopamine neurons make glutamatergic synapses in vitro, *J. Neurosci.* **18**, 4588–4602 (1998).
84. L. É. Trudeau, Glutamate co-transmission as an emerging concept in monoamine neuron function, *J. Psychiatry Neurosci.* **29**, 296–310 (2004).
85. Y. H. Joo, Y. K. Kim, I. G. Choi, H. J. Kim, Y. D. Son, H. K. Kim, P. Cumming, J. H. Kim, In vivo glucose metabolism and glutamate levels in mGluR5 knockout mice: a multimodal neuroimaging study using [18F]FDG microPET and MRS, *EJNMMI Res.* **10** (2020), doi:10.1186/s13550-020-00716-z.
86. K. Hoenig, A. Hochrein, B. B. Quednow, W. Maier, M. Wagner, Impaired prepulse inhibition of acoustic startle in obsessive-compulsive disorder, *Biol. Psychiatry* **57**, 1153–1158 (2005).

87. S. P. Whiteside, J. D. Port, J. S. Abramowitz, A meta-analysis of functional neuroimaging in obsessive-compulsive disorder, *Psychiatry Res. - Neuroimaging* **132**, 69–79 (2004).
88. J. V. Roughan, P. A. Flecknell, Behavioural effects of laparotomy and analgesic effects of ketoprofen and carprofen in rats, *Pain* **90**, 65–74 (2001).
89. S. H. Keller, E. N. L'Estrade, B. Dall, M. Palner, M. Herth, in *2016 IEEE Nuclear Science Symposium, Medical Imaging Conference and Room-Temperature Semiconductor Detector Workshop (NSS/MIC/RTSD)*, (IEEE, 2016), pp. 1–3.
90. S. H. Keller, C. Svarer, M. Sibomana, Attenuation correction for the HRRT PET-scanner using transmission scatter correction and total variation regularization., *IEEE Trans. Med. Imaging* **32**, 1611–21 (2013).
91. J. Villadsen, H. D. Hansen, L. M. Jørgensen, S. H. Keller, F. L. Andersen, I. N. Petersen, G. M. Knudsen, C. Svarer, Automatic delineation of brain regions on MRI and PET images from the pig., *J. Neurosci. Methods* **294**, 51–58 (2018).
92. W. H. Thompson, P. Fransson, On Stabilizing the Variance of Dynamic Functional Brain Connectivity Time Series, *Brain Connect.* **6**, 735–746 (2016).
93. S. Holm, A Simple Sequentially Rejective Multiple Test Procedure, *Scand. J. Stat.* **6**, 65–70 (1979).

**Acknowledgments**
Structural reference MR image is generously provided by Kristian Nygaard Mortensen, Center for Translational Neuromedicine, University of Copenhagen. Technical expertise regarding acoustic startle response and prepulse inhibition was generously provided by Kim Fejgin at H. Lundbeck. Radiochemical support was generously provided by Matthias M. Herth and Vladimir Shalgunov, Department of Drug Design and Pharmacology, University of Copenhagen. Statistical discussions with Professor Todd Ogden, Department of Biostatistics, Columbia University, NY. Professor, DM Gitte M. Knudsen, head of the Neurobiology Research Unit, Copenhagen University Hospital, offered her support and guidance for students and researchers throughout the project. **Funding:** Funding for this project was provided by the Lundbeck Foundation, Augustinus Foundation, Independent Research Fund Denmark, Savværksejer Jeppe Juhls og Hustrus Ovita Juhls Mindelegat and Købmand i Odense Johann og Hanne Weimann født Seedorffs Legat. **Competing Interest:** Mikael Palner is collaborating with the company Compass Pathways Plc (London, UK). **Data and materials availability:** LE-Tg(TH-Cre)3.1Deis rats are governed by an MTA from the NIH Rat Resource and Research Center, (MO, USA). Mikael Palner is now also employed at the University of Southern Denmark, Department of Clinical Research and Odense University Hospital, Department of Nuclear Medicine.

**Supplementary Materials**

*Chemicals*

*Viral Vectors*

*Software*

*Breeding and Phenotypic Assessment in Animals*

## Figures

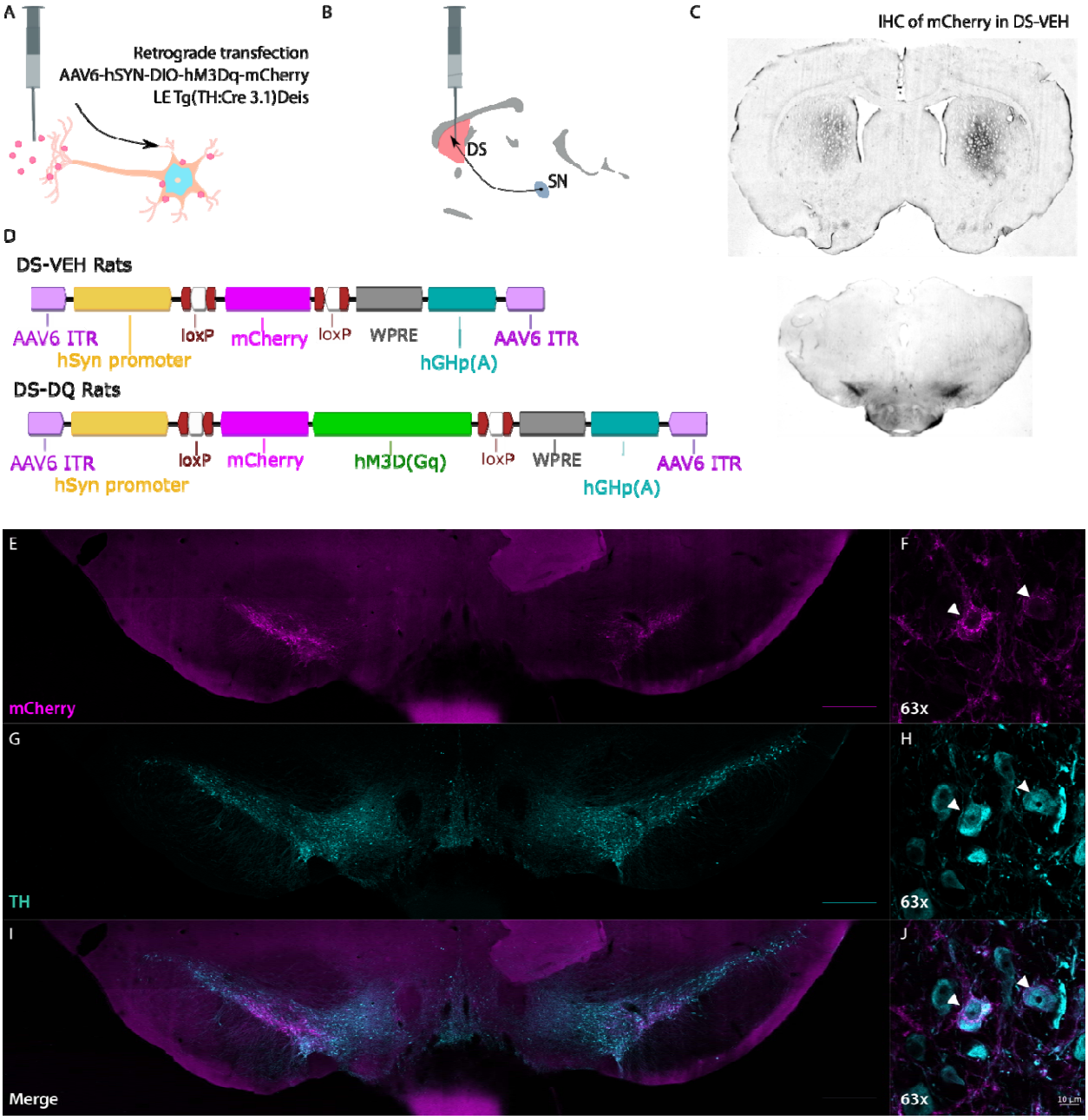


Figure 1: A,B) Retrograde transfection of Cre-positive tyrosine hydroxylase (TH) expressing neurons in the dorsomedial striatum. C) Immunohistochemical staining of mCherry in dorsomedial striatum and in substantia nigra. E) Viral vectors used in the vehicle (DS-VEH) and chemogenetic (DS-DQ) transfection groups. E-J) Fluorescent microscopy of mCherry (viral transfected) and TH-positive (dopamine) cells in the VTA and SN regions of the mesencephalon.

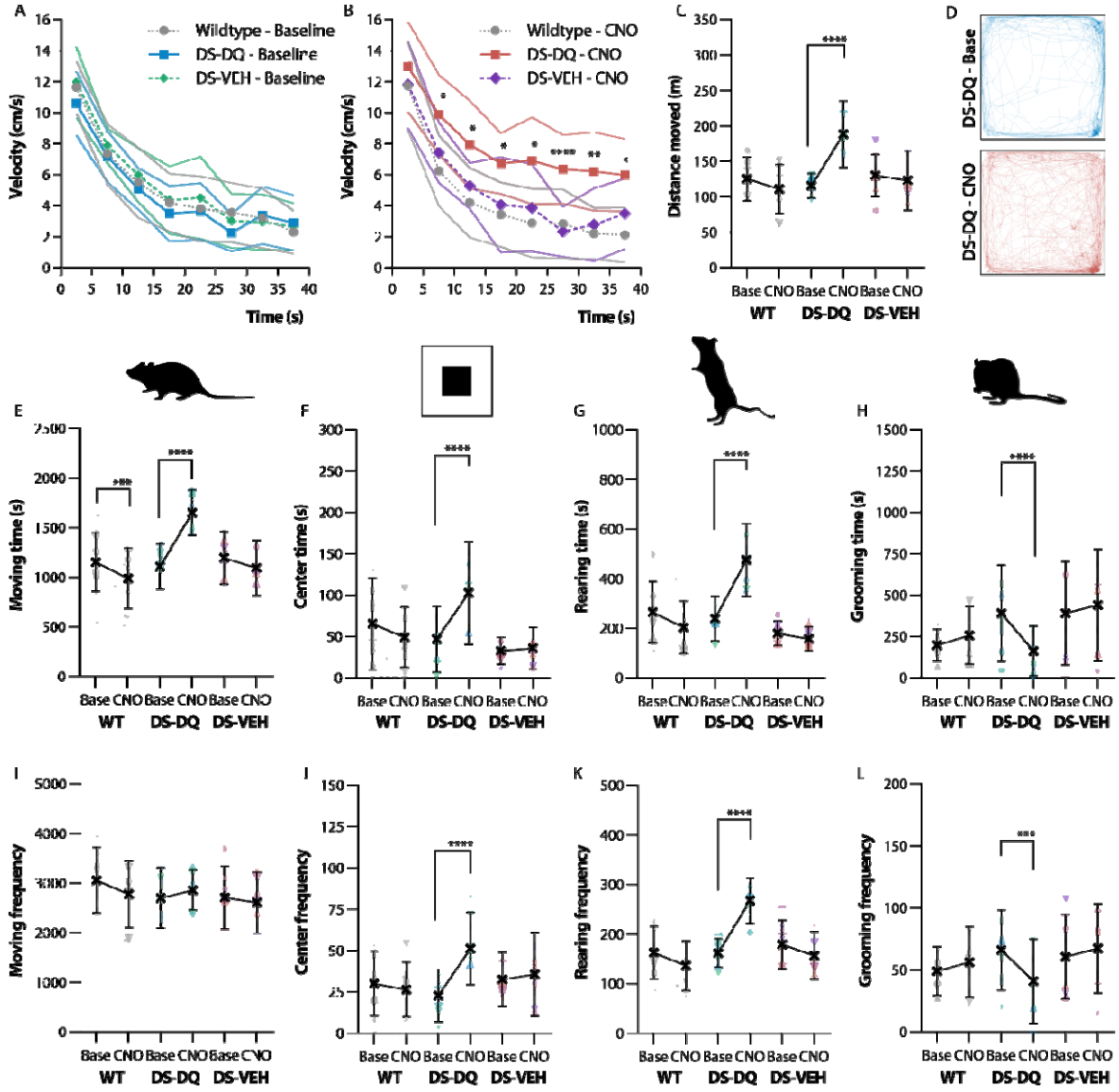


Figure 2: Open field behavior. A, B) Velocity over time as a function of time in the open field. C) Total distance traveled over the whole time course. D) Tracking of the median DS-DQ rat before and after CNO. E, F, G, H) Total time spent moving, in the center of the open field, rearing or grooming. I, J, K, L) Frequency of movement initiations, entries into the center square, rearings or grooming bouts. (♂ = ▲) (♀ =▼).

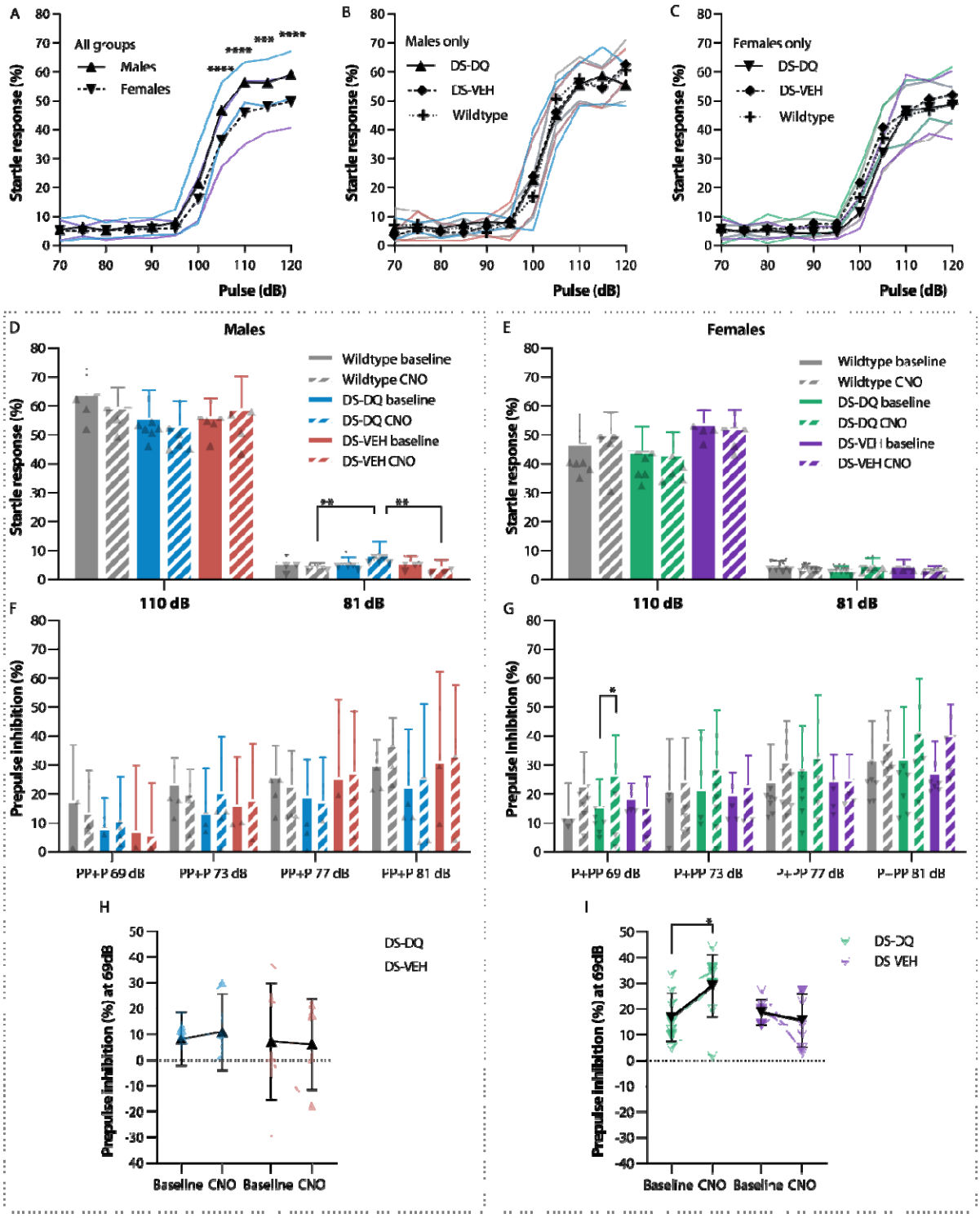


Figure 3: Acoustic startle response and prepulse inhibition. A, B, C) Startle response to various volumes of pulses. D, E) Startle response and effect of DS-DQ activation at high volume (110 dB) pulses and low volume (81 dB) prepulses. F, G) PPI as a result of prepulse intensities, negative PPI values are not shown in F and G to simplify the graph but were included in the statistical analysis. H, I) All PPI values at the lowest prepulse intensity (69 dB) pre and post CNO treatment to activate the nigro-striatal dopaminergic pathway. (♂ = ▲) (♀ =▼).

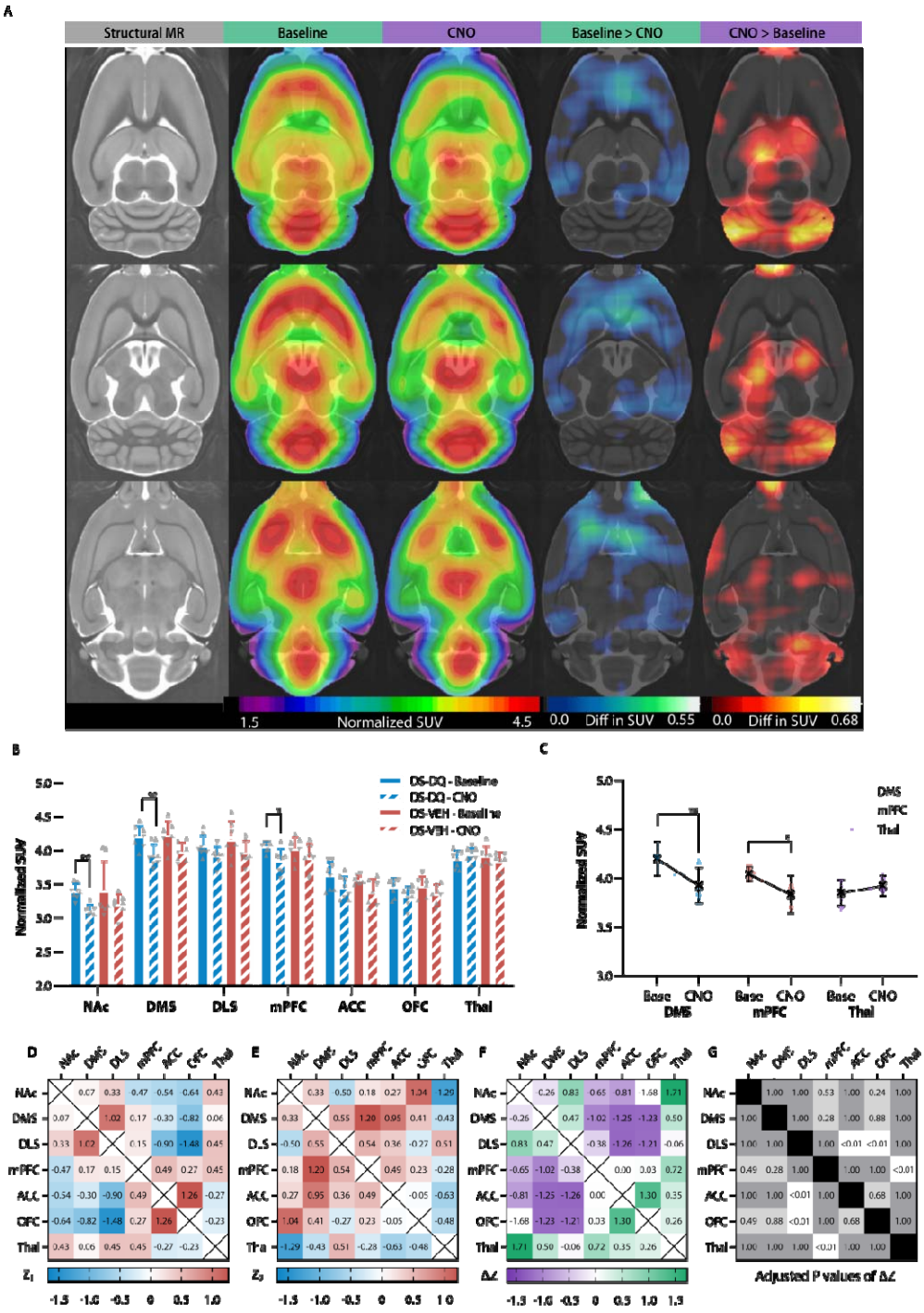


Figure 4: [$^{18}$F]FDG images and functional metabolic connectivity. A) [$^{18}$F]FDG uptake in DS-DQ animal at baseline and after chemogenetic stimulation (rainbow color), lower metabolic activity (blue color), higher metabolic activity (red color). B) Regional standard uptake values at all conditions and C) significant changes and individual animals in DMS and mPFC. D) Fisher-Z correlations in DS-DQ animals at baselines. E) Similar correlations in DS-DQ animals after chemogenetic stimulations. F) ΔZ values for each region, showing the total difference between correlations. G) Significantly changed correlations (white squares) and adjusted p-values following multiple comparison correction. (♂ = ▲) (♀ =▼).

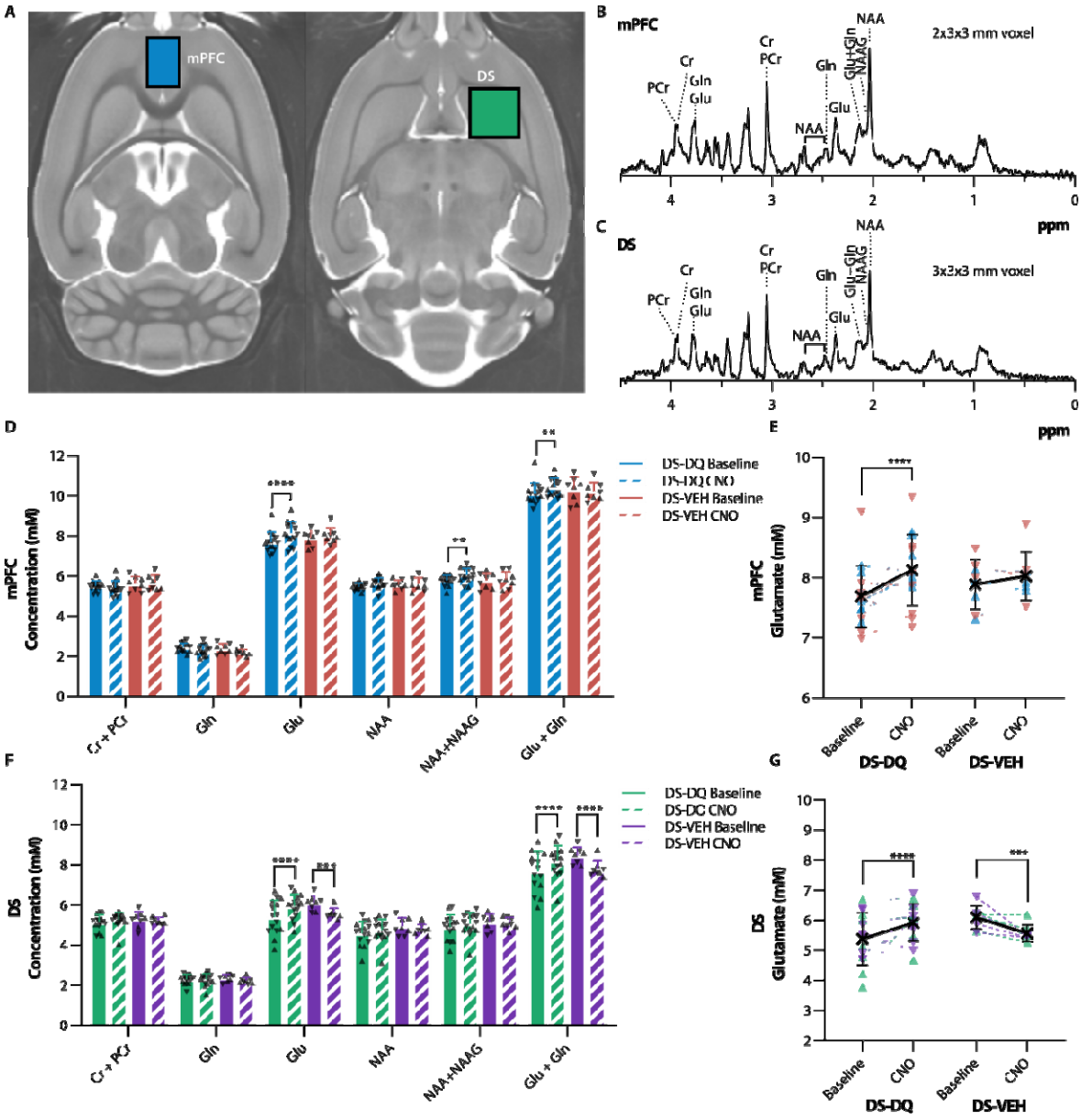


Figure 5: MR spectroscopy of neurochemicals in DS-DQ and DS-VEH animals. A) Voxel placement in mPFC (blue voxel) and DS (green voxel). B,C) Sample spectra from the mPFC and DS. D,F) Neurochemical concentrations in the mPFC in all conditions, E,G) significant changes in glutamate on the individual level. (♂ = ▲) (♀ =▼).